Convective flow reversal in self-powered enzyme micropumps

Isamar Ortiz-Rivera[a,1], Henry Shum[b,1], Arjun Agrawal[a], Ayusman Sen[a,2], and Anna C. Balazs[b,2]

[a]Department of Chemistry, The Pennsylvania State University, University Park, PA 16802; and [b]Department of Chemical & Petroleum Engineering, University of Pittsburgh, Pittsburgh, PA 15261

Edited by David A. Weitz, Harvard University, Cambridge, MA, and approved January 26, 2016 (received for review September 8, 2015)

Surface-bound enzymes can act as pumps that drive large-scale fluid flows in the presence of their substrates or promoters. Thus, enzymatic catalysis can be harnessed for "on demand" pumping in nano- and microfluidic devices powered by an intrinsic energy source. The mechanisms controlling the pumping have not, however, been completely elucidated. Herein, we combine theory and experiments to demonstrate a previously unreported spatiotemporal variation in pumping behavior in urease-based pumps and uncover the mechanisms behind these dynamics. We developed a theoretical model for the transduction of chemical energy into mechanical fluid flow in these systems, capturing buoyancy effects due to the solution containing nonuniform concentrations of substrate and product. We find that the qualitative features of the flow depend on the ratios of diffusivities $\delta = D_P/D_S$ and expansion coefficients $\beta = \beta_P/\beta_S$ of the reaction substrate (*S*) and product (*P*). If $\delta > 1$ and $\delta > \beta$ (or if $\delta < 1$ and $\delta < \beta$), an unexpected phenomenon arises: the flow direction reverses with time and distance from the pump. Our experimental results are in qualitative agreement with the model and show that both the speed and direction of fluid pumping (*i*) depend on the enzyme activity and coverage, (*ii*) vary with the distance from the pump, and (*iii*) evolve with time. These findings permit the rational design of enzymatic pumps that accurately control the direction and speed of fluid flow without external power sources, enabling effective, self-powered fluidic devices.

enzyme micropumps | solutal convection | flow reversal | self-powered systems | catalysis

Nonmechanical nano/microscale pumps that provide precise control over fluid flow without an external power source and are capable of turning on in response to specific analytes in solution are needed for the next generation of smart micro- and nanoscale devices. Specific applications involve neutralization of toxins (1), on-demand drug or antidote delivery (2), and the directed focusing of targeted analytes for optimal sensing (3). Recent experiments have shown that surface-bound enzymes act as pumps in the presence of their specific substrates or promoters, driving large-scale fluid flows (2, 4). Furthermore, fluid velocity increases with increasing reaction rate. Therefore, enzymatic catalysis provides an intrinsic energy source for fluid movement and thus can be harnessed to overcome a significant obstacle in nano- and microfluidics: the need to use pressure-driven pumps to push fluids through devices. To fully exploit this behavior, it is vital to develop a fundamental understanding of how the chemical energy is transduced into mechanical fluid flow. One possible mechanism involves thermal buoyancy effects: An exothermic reaction catalyzed by the enzyme lowers the solution density, causing fluid to be drawn in and rise above the pump (Fig. 1*A*). Not all observed pumping, however, can be explained by this mechanism. In several instances (4), the thermal input from the enzymatic reaction is far lower than that required to generate the observed pumping velocity. Even more remarkable is the observation that urease-based pumps generate flows that are in the opposite direction to that expected for thermally driven movement (2). One possible explanation involves a reaction-induced net increase in solution density, through changes in solutal composition, rather than a net decrease due to heat release (Fig. 1*B*). Herein, we examine the anomalous flow pattern for the urease pump and, by developing a theoretical model, we show that the flow pattern depends on the relative diffusivities and expansion coefficients of the reactants and products. Furthermore, we isolate conditions where the system exhibits a previously unobserved phenomenon: a pronounced reversal in the flow direction. Our experiments confirm the latter prediction and demonstrate that both the speed and direction of fluid pumping (*i*) depend on the enzyme activity and coverage, (*ii*) vary with the distance from the pump, and (*iii*) evolve with time. These findings allow us to rationally control fluid flow for the directed delivery of payloads to designated locations in microchambers.

Results and Discussion

Modeling and Simulation.

Reaction-induced mechanisms for driving fluid flow. To ascertain how chemical reactions at the enzyme pump contribute to the fluid flows, we assess the relative strengths of the following effects: diffusioosmosis, thermal buoyancy, solutal buoyancy, and thermodiffusion (Soret effect).

Diffusioosmosis is the flow of water along a charged, fixed surface caused by tangential gradients in concentrations of either charged or uncharged solute (5, 6). Due to the diffusioosmotic effect, concentration gradients around dissolving salt particles (7, 8) can drive the radial motion of tracer particles at speeds of ~10 μm/s, which is similar in order of magnitude to the flows observed from enzyme pumps (2). Notably, the motion of a particle due to solute concentration gradients near a wall is a combination of the diffusioosmotic fluid flow u^{DO} along the fixed wall and diffusiophoretic motion of the particle relative to the fluid flow, v^{DP}, both of which are proportional to the quantity $\nabla C/C$, where C is the solute concentration (5, 7). Near an impermeable

Significance

Surface-bound enzymes act as pumps in the presence of their specific substrates or promoters, thereby combining sensing and fluidic pumping into a single self-powered microdevice. Using a combination of theory and experiments, we have elucidated the mechanism of the prototypical urease-based pump. We find that even simple enzymatic reactions can drive complex, time-dependent flows whose direction and speed depend critically on the relative diffusivities and expansion coefficients of the reactants and products. Our approach allows us to accurately predict the behavior of new pump designs under different conditions.

Author contributions: I.O.-R., H.S., A.S., and A.C.B. designed research; I.O.-R., H.S., and A.A. performed research; A.S. contributed new reagents/analytic tools; I.O.-R., H.S., A.A., A.S., and A.C.B. analyzed data; and I.O.-R., H.S., A.S., and A.C.B. wrote the paper.

The authors declare no conflict of interest.

This article is a PNAS Direct Submission.

[1]I.O.-R. and H.S. contributed equally to this work.

[2]To whom correspondence may be addressed. Email: balazs@pitt.edu or asen@psu.edu.

This article contains supporting information online at www.pnas.org/lookup/suppl/doi:10.1073/pnas.1517908113/-/DCSupplemental.

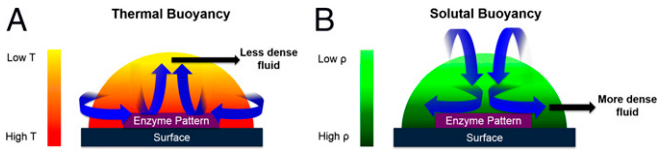

Fig. 1. Possible mechanisms of fluid convection in enzyme-powered micropumps. The fluid flow observed in enzyme-powered micropumps in the presence of substrate has been attributed to two factors: (*A*) thermal buoyancy and (*B*) solutal buoyancy. Exothermic enzymatic reactions heat the fluid, lowering solution density and causing fluid to be drawn in and rise above the pump (*A*). Solutal buoyancy effects arise from the differences in density between the reactants and the products of an enzymatic reaction. Converting reactants to products can either decrease the density of the solution at the pattern surface, which drives flows as in *A*, or increase the density, which drives convective flows in the opposite direction as in *B*.

wall, the concentration gradients are parallel to the wall and, due to radial symmetry of the enzyme patch, would cause tracer particles to move either toward or away from the pump. Inverting the pump setup (so that the enzyme patch is now on the top wall of the chamber) does not affect the direction of lateral concentration gradients so the direction of tracer motion should remain unchanged. In experiments, however, tracer particles near the surface bearing the enzyme patch moved in the opposite direction relative to the patch when the setup was inverted (2). Thus, we conclude that diffusioosmosis is not the dominant driving mechanism for the flow in these pump systems (2).

The observation that the direction of pumping was reversed when the chamber was inverted is strongly indicative of buoyancy effects, which depend on the direction of the gravitational force. Sengupta et al. (2) numerically showed that temperature gradients generated by the reaction (assuming the reaction rate $F = 10^{-7}$ mol·s^{-1} and enthalpy of reaction $\Delta H = -100$ kJ·mol^{-1}) could lead to convective flow speeds of around 1 μm/s toward the patch in the normal setup; this value is similar in order of magnitude for several different enzymes. An exception, however, is the urease-based pump, which catalyzes an exothermic reaction yet generates flows in the opposite direction, i.e., away from the patch in the normal setup, consistent with a reaction-induced increase of fluid density at the pump (2). To explain this behavior, it was hypothesized that the reaction product was denser than the initial urea solution (Fig. 1*B*) and this solutal buoyancy effect was larger than the density decrease due to exothermicity.

Indeed, a rough calculation shows that solutal density effects dominate over thermal effects. For small changes in solute concentration S and temperature T, the fluid density can be approximated by (9) $\rho = \rho_0(1 + \beta_S(S - S_0) - \beta_T(T - T_0))$, where ρ_0 is the density at a reference point with temperature T_0 and solute concentration S_0. The volumetric expansion coefficients β_S and β_T measure the sensitivity of the fluid density to changes in concentration and temperature, respectively. For a localized (point-like) reaction occurring at rate F, the steady-state temperature and substrate concentration fields in an unbounded 3D environment are respectively $T = T_\infty - (1/4\pi r)F\Delta H/D_T c_p \rho_0$ and $S = S_\infty - (1/4\pi r)F/D_S$, where r is the distance from the reaction, D_T is the heat diffusivity, D_S is the solute diffusivity, ΔH is the enthalpy of the reaction (negative for exothermic reactions), and c_p is the constant-pressure specific heat capacity of the fluid. The ratio of temperature to concentration gradients is then $\partial_r T/\partial_r S = D_S \Delta H/D_T c_p \rho_0$. The notation $\partial_r = \partial/\partial r$ signifies the spatial derivative in the radial direction. The influence of thermal buoyancy relative to solutal buoyancy is indicated by the ratio of their Rayleigh numbers,

$$\frac{\mathrm{Ra}_T}{\mathrm{Ra}_S} = \frac{\beta_T \partial_r T}{\beta_S \partial_r S} = \frac{\beta_T D_S \Delta H}{\beta_S D_T c_p \rho_0}. \qquad [1]$$

We consider the solute to be urea and the reaction to be the hydrolysis of urea by urease ($\Delta H = -59.6$ kJ · mol^{-1}) (10). Using known physical properties of water and urea (11), we obtain $\mathrm{Ra}_T/\mathrm{Ra}_S \approx 0.002$ and thus the small thermal effects can be neglected for the urease-based pump. This suggests that solutal buoyancy plays a dominant role, and factors like the differential diffusion of substrate and product species should be considered.

With respect to thermodiffusion (the Soret effect), it is known that temperature gradients can contribute to the diffusive flux of solute, which for dilute solutions is (12)

$$J_r = -D_S[\partial_r S + (\sigma + \beta_T)S \cdot \partial_r T], \qquad [2]$$

where σ is the Soret coefficient and other variables are as defined above. In the absence of temperature gradients, this expression yields the usual Fickian diffusive flux. The magnitude and sign of the Soret coefficient depend on factors such as the solute size, background salt concentration, and temperature (13, 14). The Soret coefficient is typically positive, resulting in solute migration toward lower temperatures. Hence, solute becomes depleted in hot regions, driving fluid convection. This combination of repulsion and convection can be harnessed to trap DNA by laser heating (13). We assess the relative influence of the Soret effect in our system by the ratio of contributions from thermal gradients and solutal gradients in Eq. **2**, $J_r^T/J_r^S = (\sigma + \beta_T)S \cdot \partial_r T/\partial_r S$. Using estimates for temperature and concentration gradients from above and the Soret coefficient $\sigma = 8.1 \times 10^{-4}\mathrm{K}^{-1}$ (for urea at concentration $S = 0.417$ M) (14), this ratio is $J_r^T/J_r^S \approx 6 \times 10^{-8} << 1$. Hence, we neglect thermodiffusion for our model of the urease pump.

Model for double diffusive solutal convection pumps. Below, we argue that the interplay of the relative diffusivities and expansion coefficients of the reaction substrate S and product P gives rise to temporally and spatially complex fluid flow. In our model, we consider a shallow, fully enclosed chamber of width $2L$ in the horizontal (x and z) directions and height H in the y direction (Fig. 2). Enzymes are bound to a circular patch of radius R at the center of the bottom wall and occupy a volume of fluid of depth h above the patch; in this volume, the reaction $S \to P$ converts substrate to product with a reaction rate per unit volume f. We consider only constant reaction rates; this assumption is valid if the reaction rate is low enough that substrate depletion is insignificant over time scales of interest.

For nondimensionalization, we define the characteristic length scale $l^* = R$, time scale $t^* = R^2/D_S$, and concentration scale $S^* = P^* = f\, t^* h/H$, where D_S is the diffusion coefficient of the substrate. For the urease-based pumps in our experiments, the length and time scales correspond to $l^* \approx 3$ mm and $t^* \approx 100$ min, respectively. The dimensionless advection–reaction–diffusion equations are

$$\partial_t S + \mathbf{u} \cdot \nabla S = \nabla^2 S - \chi_E, \quad \partial_t P + \mathbf{u} \cdot \nabla P = \delta\, \nabla^2 P + \chi_E, \qquad [3]$$

where $\partial_t = \partial/\partial t$, the parameter $\delta = D_P/D_S$ is the ratio of the product diffusion coefficient D_P to the substrate diffusion coefficient D_S, and χ_E is the characteristic function, which takes the value 1 inside the volume occupied by enzymes and the value 0 outside. No-flux boundary conditions are used for the substrate and product. The chamber is initially filled uniformly with the enzyme's substrate at concentration $S(t = 0) = S_0$ and contains no product, $P(t = 0) = 0$.

Writing the change in substrate concentration (relative to the initial, homogeneous value) $\Delta S = S - S_0$ and the change in product concentration $\Delta P = P - P_0 = P$, we use the linear model for the

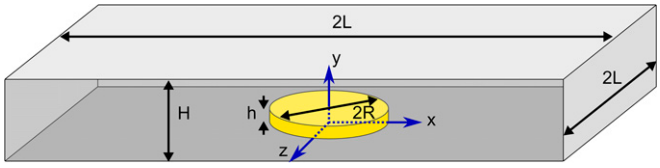

Fig. 2. Geometry for enzyme-powered microfluidic pumps used in simulations. Volume occupied by enzymes tethered to a circular patch at center of lower wall is marked in yellow.

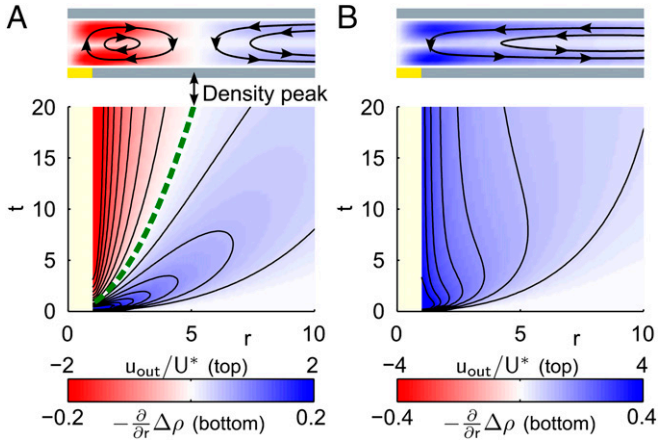

Fig. 3. Calculated evolution of the density gradient over time and resulting simulated flow field for two combinations of δ and β. (*A* and *B*, *Top*) Side view of flow fields showing streamlines at time $t = 20$ (all variables in dimensionless units) computed using the full 3D Navier–Stokes–Boussinesq model with chamber height $H = 2$ and large width $2L = 80$ (approximating a horizontally infinite domain). The color map indicates the local outward radial flow, normalized by a characteristic speed U* (defined in *SI Materials and Methods*). The enzyme reaction occurs in a thin layer above the yellow boxes at the bottom left of the cross-sections. (*A* and *B*, *Bottom*) Evolution of density gradient field $(-(\partial/\partial r)\Delta\rho)$ over time using the simplified, point source model. The dashed green curve in *A* tracks the position of the density peak over time (see *SI Materials and Methods* for a formula for this curve). Because the point source approximation is not accurate at short distances, the region $r < 1$ is omitted. Parameters are (*A*) $\delta = 2$, $\beta = 1.7$ and (*B*) $\delta = 1.7$, $\beta = 2$.

dimensional fluid density (9), $\rho = \rho_0(1 + \beta_S\Delta S + \beta_P\Delta P) = \rho_0(1 + \Delta\rho)$, where ρ_0 is the initial, uniform fluid density and $\Delta\rho = \beta_S\Delta S + \beta_P\Delta P$ is the fractional change in density due to changes in solute composition. The constants β_S and β_P are the volumetric coefficients of expansion due to the substrate and product, respectively. Positive values of β_S and β_P indicate that fluid density increases with solute concentration, as is commonly the case. Defining the parameter $\beta = \beta_P/\beta_S$ and rescaling the density by $\rho^* = \rho_0\beta_S S^*$, the dimensionless equation for density is $\rho = \rho_0 + \Delta\rho$, $\Delta\rho = \Delta S + \beta\ \Delta P$.

Following the Boussinesq approximation (15), the fluid flow $\mathbf{u}$ is governed by the incompressible Navier–Stokes equations with a buoyancy force term. We use the length and time scales as above and define the velocity scale $u^* = l^*/t^*$ and pressure scale $p^* = \mu/t^*$, where μ is the dynamic viscosity of the fluid. The dimensionless Navier–Stokes equations driven by buoyancy forces are

$$\mathrm{Sc}^{-1}(\partial_t\mathbf{u} + \mathbf{u}\cdot\nabla\mathbf{u}) = -\nabla p + \nabla^2\mathbf{u} - \mathrm{Ra}\cdot\Delta\rho\ \mathbf{e}_y, \quad \nabla\cdot\mathbf{u} = 0, \qquad [4]$$

where $\mathrm{Sc} = \mu/\rho_0 D_S \sim 1{,}000$ is the Schmidt number. The buoyancy force term in Eq. **4** is proportional to the rescaled density change $\Delta\rho = \Delta S + \beta\,\Delta P$, and the characteristic strength of convection is determined by the Rayleigh number, $\mathrm{Ra} = \rho_0 g\ \beta_S R^5 f\ h\ (\mu\ D_S^2 H)^{-1}$, where g is the acceleration due to gravity. In Eq. **4**, we have omitted the uniform buoyancy force proportional to ρ_0 because any constant force can be incorporated into the pressure gradient term by considering a modified pressure field. We impose no-slip boundary conditions for the fluid and assume that the fluid is initially at rest, $\mathbf{u}(\mathbf{x}, t = 0) = \mathbf{0}$.

Our modeling approach is similar to that in prior reaction–diffusion–convection studies (16–18), except that we confine the reaction to a finite region containing bound enzymes. To the best of our knowledge, the latter setup has not been treated theoretically, but has clear relevance to the function of enzyme-driven pumps, as well as mixing in microfluidic reaction chambers.

In general, we expect buoyancy effects to cause fluid to either rise or sink above the enzyme patch, driving toroidal convection rolls. Such flow patterns were described in previous experiments with enzyme pumps (2, 4) and have also been induced by localized heating in thin layers of oil (19). In the case of sinking fluid, resulting from a local increase in density, fluid is pushed out radially away from the pump at the bottom of the chamber and drawn in radially at the top of the chamber. We refer to this as "outward" pumping. Conversely, "inward" flow moves toward the pump along the bottom and spreads radially outward at the top of the chamber. To quantify the characteristics of the flow, we define the outward flow at a point in the chamber,

$$u_{\mathrm{out}}(x,y,z) = \begin{cases} \mathbf{u}(x,y,z)\cdot\mathbf{e}_r, & \text{if } y < H/2, \\ -\mathbf{u}(x,y,z)\cdot\mathbf{e}_r, & \text{if } y > H/2, \end{cases} \qquad [5]$$

where $\mathbf{e}_r = (x, 0, z)^{\mathrm{T}}/\sqrt{x^2 + z^2}$ is a unit vector in the radial direction. We also define the vertically averaged outward radial flow,

$$\overline{u}_{\mathrm{out}}(x,z,t) = \frac{1}{H}\int_0^H u_{\mathrm{out}}(x,y,z,t)\,\mathrm{d}y, \qquad [6]$$

which is positive for flow in the outward sense and negative for inward flow, as described above. Hence, inward flow could be quantified by $\overline{u}_{\mathrm{in}} = -\overline{u}_{\mathrm{out}}$.

Because the Schmidt number is large, the inertial terms in the Navier–Stokes equations (Eq. **4**) may be neglected, resulting in Stokes flow. The fundamental solution of Stokes flow driven by a point force acting between infinite, parallel plates is known (20). Each small volume element of fluid exerts a point-like buoyancy force, driving a toroidal flow (Fig. S1). This clearly demonstrates that horizontal (as well as vertical) fluid flows are generated by vertical forces. Summing up contributions from each volume element, we find that the net radial flow produced by the pump is approximately proportional to radial changes in fluid density in the chamber, $\overline{u}_{\mathrm{out}} \sim -(\partial\rho/\partial r)$ (*SI Materials and Methods*). By

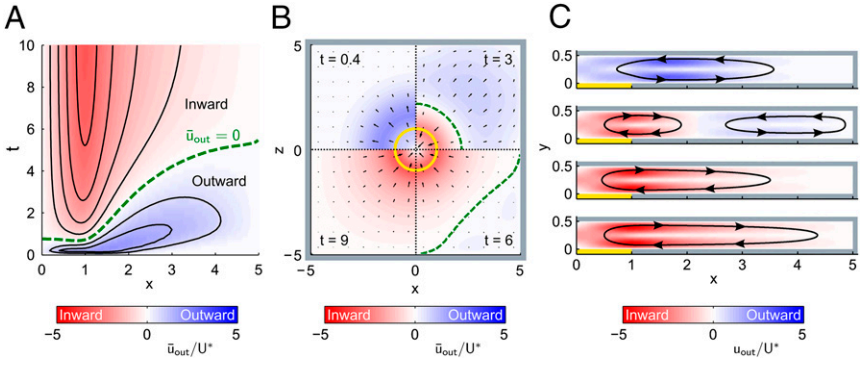

Fig. 4. Simulated spatiotemporal flow field evolution illustrating flow reversal in an enclosed chamber. (*A*) Outward flow $\overline{u}_{\mathrm{out}}$ (Eq. **6**) as a function of time and distance from the pump center. The scaling factor U* is defined in *SI Materials and Methods*. (*B*) Top (*x*–*z*) view of the chamber with snapshots at different times in each quadrant, as labeled. Arrows indicate flow in the bottom half of the chamber. The perimeter of the enzyme patch is shown by the yellow circle. (*C*) Side views of the flow at the same times as in *B*, increasing from top to bottom. The cross-sections are at $z = 0$ and only the right half ($x \geq 0$) is shown. Parameters are $L = 5$, $H = 0.5$, $\delta = 2$, and $\beta = 1.7$. Movie S1 shows the flow field in the bottom half of the chamber.

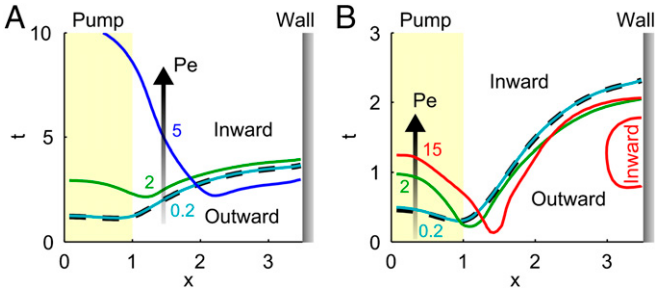

Fig. 5. Advection–diffusion–reaction simulations for transitions from outward to inward pumping at various Péclet numbers (Pe). We calculate Pe in these simulations according to Eq. **S11** (*SI Materials and Methods*). For each value of Pe, the region below the curve exhibits outward flow and the region above the curve exhibits inward flow. The Pe = 15 (red) case in *B* has an additional region of inward flow, as labeled. The dashed curves (underlying the Pe = 0.2 curves) correspond to the Pe = 0 limit (chemical advection disabled in simulations). The expansion coefficient ratios are (*A*) $\beta = 1.08$ and (*B*) $\beta = 1.05$. Other simulation parameters are: $L = 3.5$, $H = 0.5$, and $\delta = 1.1$.

deriving an expression for the density field (treating the pump as a point source of product and point sink of substrate—see *SI Materials and Methods* for details), we can use the above relationship to predict the flow field near the pump.

Analysis revealed unexpectedly rich behavior of the flow field that depends on δ and β: The direction of flow can reverse over time and depends on the distance from the pump. Assuming $\delta = D_P/D_S > 1$ (as for the urease pump), this behavior occurs if $\delta > \beta (= \beta_P/\beta_S)$. Here, a wave of high-density fluid propagates radially from the pump; the flow near the pump will be inward and the flow far from the pump (beyond the peak in density) will be outward (Fig. 3*A*). Flow reversal is also predicted for $\delta < 1$ if $\delta < \beta$, but now flow is in the opposite direction, driven by a wave of low-density fluid. For all other combinations of δ and β, the fluid flow direction (outward if $\beta > 1$, inward if $\beta < 1$) will not vary with time or position. Density profiles for various combinations of δ and β are depicted in Fig. S2.

Fig. 3 shows the temporal evolution of the density gradient $(-(\partial/\partial r)\Delta\rho)$ computed from the point source model in an infinite 2D domain and the flow structure obtained from full 3D simulations of the Navier–Stokes–Boussinesq model. The plots support the predicted correlation between the density gradient and the flow field (Fig. S3). Fig. 3*A* shows the predicted flow reversal when $\delta > 1$ and $\delta > \beta$; the peak in the density lies at a finite distance from the pump, giving rise to inward flow on the left and outward flow on the right. In contrast, when $\delta < \beta$ (Fig. 3*B*), the fluid density is greatest at the enzyme patch ($r = 0$) and decreases monotonically with distance, leading to outward flow everywhere.

Having uncovered the fundamental process of flow reversal, we performed simulations with the patch size and chamber aspect ratio approximating the experimental setup (*Experimental Observations*) for $\delta > 1$ and $\delta > \beta$. Fig. 4 shows three distinct periods in the flow evolution. At early times, flow is in the outward direction throughout the chamber. At late times, flow is in the inward direction throughout. At intermediate times, there is an expanding inner region of inward flow and a coexisting outer region with outward flow.

We also performed simulations taking into account the chemical advection terms in Eq. **3**. These nonlinear effects are expected to be negligible if the Péclet number, which is proportional to the Rayleigh number, is small, but may become significant if the reaction rate is high, for instance. With the simulation parameters $\beta = 1.08$ and $\delta = 1.1$ (Fig. 5*A*), we found that increasing the Péclet number delayed the onset of the outward-to-inward flow reversal at positions close to the pump. Fig. 5*B* (Pe = 15, red curve) demonstrates that at high Pe, the emergence of additional flow direction transitions is possible; a small region of inward flow transiently appears close to the side wall.

The examples in Fig. 5 indicate that the effects of increasing Pe depend on model parameters. In these examples, the dynamics are particularly sensitive to parameter values because $\beta \approx \delta$, which means the system is near the critical point for flow reversal. The time of first appearance of inward flow varies from $t \approx 0.15$ (Fig. 5*B*, Pe = 15) to $t \approx 2$ (Fig. 5*A*, Pe = 5), corresponding to 15–200 min. The nonlinear dependence of the flow on reaction rate (via Pe) and physical parameters suggests further possibilities for designing complex flow patterns using enzymatic pumps. By choosing reactions with suitable values of δ and β and controlling the rate of reaction, it is possible to tailor the flow characteristics.

Experimental Observations.

Fabrication of enzyme pumps. Enzyme-powered pumps were fabricated as follows (Fig. S4). A gold (Au) patch (6 mm diameter) was patterned on a polyethylene glycol (PEG)-coated glass surface. A biotin thiol linker was then added to form a self-assembled monolayer (SAM) on the Au patch, followed by the addition of streptavidin. Enzyme attachment on the streptavidin-functionalized surface was then attained via a protein–ligand linkage, facilitated through a biotin tag. Enzyme coverage on the patch was varied by changing the enzyme concentration in the solution used to prepare the pattern. The fabrication was completed by placing a spacer (20 mm diameter, 1.3 mm height) on top of the enzyme-patterned surface to seal the chamber and create a closed system. A buffered solution of substrate with suspended tracer particles (2 μm in size) was injected into the

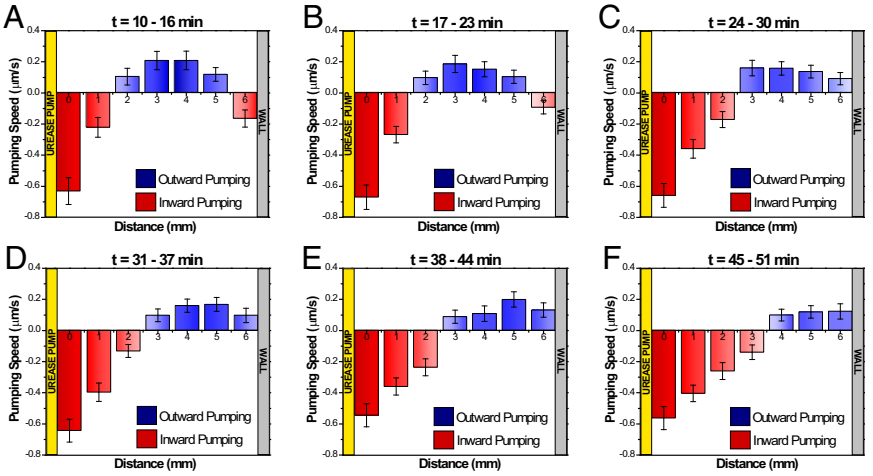

Fig. 6. Experimentally obtained spatiotemporal pumping behavior of urease-powered pumps at low enzyme coverages. The pumping speeds of urease-powered pumps containing low enzyme coverage were measured as a function of distance at different time intervals. The urease enzyme concentration used for soaking the functionalized gold patch was 3×10^{-9} M. (*A*) Initially there was inward pumping close to the pump, whereas farther away, a region of outward pumping was observed (*B*–*F*). With time, the region of inward pumping extended farther away from the pump, as the outward pumping regime was diminished. The means and SDs are calculated for 30 tracer particles. See Table S1 for data. See Fig. S5 for pumping speeds as a function of time at different distances away from the enzyme pump. See Table S2 for data.

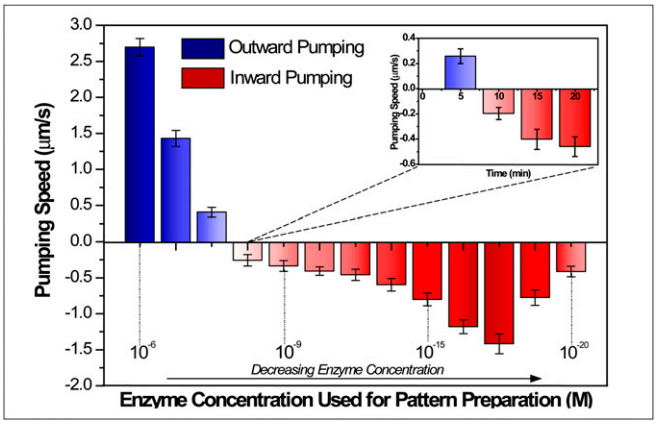

Fig. 7. Pumping speeds of urease-powered micropumps as a function of enzyme coverage. The pumping speeds of urease-powered pumps were measured as a function of the concentration of biotin-tagged urease in the solution used for soaking the biotin–streptavidin functionalized Au patch. Lower concentrations of soaking solution result in less enzyme immobilized on the patch. The speed and direction of fluid flow near the pump were monitored after 20 min of pump activation in the presence of 500 mM urea in 10 mM PBS. At higher enzyme coverages, only outward pumping (i.e., away from the patch) was observed. As the enzyme coverage was lowered, the fluid flow direction was reversed, and inward pumping was observed. (*Inset*) Pumping speeds over time for an intermediate enzyme coverage show outward pumping at early times and inward pumping at late times, as predicted by the theoretical model. The means and SDs shown are calculated for 30 tracer particles (Tables S3 and S4).

chamber and the fluid flow was monitored with an optical microscope.

Experimental results. Experiments were performed on urease micropumps to test the predictions that the system exhibited an initial outward flow, which was later replaced by an inward flow region that developed at the vicinity of the pump and spread farther away with time. Movies of tracer particles were analyzed to measure the pumping speeds induced by the pump as a function of distance at different time intervals from the introduction of urea solution (Fig. 6). The urease concentration used for soaking the functionalized gold patch was 3×10^{-9} M. As shown, initially (during the first time interval) there was inward pumping close to the pump, whereas farther away a region of outward pumping was seen. With time, the region of inward pumping gradually extended farther away from the pump. The observations are in close agreement with the theoretical model, confirming the role of solutal buoyancy in the pumping mechanisms and validating the theoretical approach. We also note that a small region of inward flow is observed transiently at the perimeter of the chamber (Fig. 6 *A* and *B*). This structure is not predicted by our linear theory but was observed in simulations with large Pe effects (Fig. 5*B*).

To investigate the pumping behavior as a function of enzyme coverage, biotin–streptavidin functionalized Au surfaces were exposed to solutions containing different concentrations of biotin-tagged urease. At higher enzyme coverages, only outward pumping (i.e., away from the patch) was observed close to the pump after 20 min (Fig. 7). As the enzyme coverage was lowered, resulting in lower reaction rates, the fluid flow direction reversed, and inward pumping was observed. This fluid flow reversal occurs gradually as a function of enzyme concentration. The maximum observed inward pumping speed was around half the magnitude of the maximum observed outward speed. Further decreasing the enzyme coverage resulted in a reduction in magnitude of inward pumping, consistent with the scaling argument that, for low reaction rates, the flow speed is proportional to the rate of reaction (*SI Materials and Methods*). Flow reversal with time was verified over an intermediate range of enzyme coverage (Fig. 7, *Inset*): Outward pumping was observed initially, but was replaced by inward pumping over time.

The observed dependence of pumping direction (at a fixed position and time) on enzyme coverage is consistent with simulation results in Fig. 5*A* for flows at different Péclet numbers. The transition from outward to inward flows near the pump was delayed as Pe (approximate reaction rate) was increased. Hence, at a fixed time it is possible that a low-enzyme pump has transitioned to inward pumping whereas a high-enzyme pump is still producing an outward flow, as we observe experimentally.

Experimental parameter estimates. To quantify the change in solution density due to the enzyme catalyzed reaction, we compared the densities of a solution of urease and urea before and after reaction (details in *SI Materials and Methods* and Table S5). The estimated ratio of expansion coefficients was $\beta \approx 1.19 \pm 0.08$. To estimate δ, we consider the conversion of urea, $CO(NH_2)_2$, into ammonium bicarbonate (NH_4^+ and HCO_3^- ions) and obtain diffusion coefficients for the relevant species from the literature (11). The substrate diffusivity is $D_{CO(NH2)2} = 1.38 \times 10^{-5}$ cm^2/s and the product diffusivity is $D_{NH4\ HCO3} = 1.48 \times 10^{-5}$ cm^2/s (based on the effective diffusivity for a salt with $D_{NH4+} = 1.96 \times 10^{-5}$ cm^2/s and $D_{HCO3-} = 1.19 \times 10^{-5}$ cm^2/s). From these values, the ratio of diffusivities is $\delta = 1.07$.

The estimated values of δ and β are similar in magnitude. Although they do not satisfy the theoretical condition for flow reversal ($\delta > \beta$, given $\delta = 1.07$), plausible errors in the parameter estimates could mean that the true values do satisfy this condition. The expansion coefficient ratio is difficult to determine accurately because the relative increase in solution density due to the reaction is small (~1%). Diffusion coefficients reported in the literature are also often in poor agreement (11).

Conclusions

We used a combination of theory and experiments to uncover the mechanism behind the remarkable spatiotemporal variations in pumping in urease-based pumps. Having ruled out several mechanisms, we formulated a model that accounts for buoyancy effects due to nonuniform concentrations of substrate and product that have different diffusivities and volumetric expansion coefficients. We find that the qualitative features of the flow depend on the ratios of diffusivities $\delta = D_P/D_S$ and expansion coefficients $\beta = \beta_P/\beta_S$ of the reaction substrate and product. If $\delta > 1$ and $\delta > \beta$ (or if $\delta < 1$ and $\delta < \beta$), then the flow direction reverses with time and distance from the pump. At any given position, the flow direction at later times can be opposite to that at earlier times, and within a certain range of time, the flow direction near the pump can be opposite to that far from the pump. Numerical simulations showed that chemical advection at large Péclet numbers could delay the reversal or otherwise alter the flow pattern. Experimental results clearly confirmed the validity of our model, providing an example where the flow near the pump is initially in the outward direction but changes to inward pumping over time. The region of inward pumping then gradually spreads farther out in space, replacing outward pumping in the entire system. These findings are unexpected and surprising as previous experiments with several enzyme micropumps have seen flow speeds only decay over time as substrate is consumed (2). Here, however, we show that the flow direction can change over tens of minutes.

Our work clearly illustrates that a simple chemical reaction of the form $S \rightarrow P$ catalyzed by a patch of immobilized enzymes can drive a complex, time-dependent flow. The balance between inward convective flow, driven by substrate depletion at the pump, and outward flow, driven by product formation at the pump, can result in flow reversal if the substrate and product have different diffusivities and different expansion coefficients satisfying the conditions above. As demonstrated in experiments, this flow reversal is observable even with small differences in diffusivity and expansion coefficients. We therefore expect that many other reaction systems can exhibit similar behavior.

We showed that, for low reaction rates, the flow induced by these enzymatic pumps is roughly proportional to the local horizontal gradients in fluid density and could therefore be predicted from a

simple 2D model for the density evolution. Such a density field can be computed quickly, using fundamental solutions of the diffusion equation, whereas simulation of diffusion and advection in 3D domains is computationally demanding. Hence, our approach enables rapid evaluation of the behavior of new pump designs under different conditions. For example, flows due to multiple patches with differing enzyme loadings and arranged arbitrarily in the chamber can be predicted with our technique. Moreover, thermal effects can be incorporated in a similar manner, treating heat as one of the reaction products.

More accurate quantitative predictions of pumping can be achieved by extending the model to include the effects of substrate depletion on the rate of reaction (e.g., Michaelis–Menten kinetics) and cross-diffusion terms (the flux of a chemical species due to concentration gradients of another species; this flux can be significant in some systems) (21). Because the overall flow is sensitive to small changes in substrate and product concentration profiles, these nonlinear terms may affect the overall pumping behavior if the reaction rate is sufficiently high. We can also model more complex situations, such as oscillatory or sequential activation of pumps that could be engineered with multiple enzyme types interconnected by reaction pathways.

Materials and Methods

Numerical Methods. The finite difference method was used to numerically solve the advection–diffusion–reaction equations governing concentration fields (Eq. **3**), with second-order finite differences used for the Laplace operator and the first-order upwind scheme used for the advective term when we investigated the effects of finite Péclet number. The reaction term was implemented as a source contribution in the grid cells occupied by the patch. Because our model assumes a constant reaction rate, it is possible for substrate concentrations to become negative over the course of a simulation. We therefore verified in all simulations that the concentration changes remained small, justifying our assumption of constant reaction rates. The fluid flow was simulated using the lattice Boltzmann method (22, 23) with the D3Q19 scheme. The buoyancy force, defined in Eq. **4**, was implemented as a body force acting at each grid point (24). Bounce-back rules were adopted to enforce the no-slip boundary conditions. This combination of finite difference and lattice Boltzmann methods has proved to be effective in modeling advection–diffusion processes (25, 26).

Biotinylation of Enzymes (27). A urease [*Canavalia ensiformis* (Jack bean)] (Sigma Aldrich) solution (2 mg/mL) was prepared with 100 mM PBS as the buffer. Before completing the total volume of the enzyme solution, 10 μL of a 0.1-mM 3-(*N*-maleimidylpropionyl) biocytin (Santa Cruz Biotechnology) biotin solution was added per mL of enzyme solution to get a ratio of 4:1 enzyme:biotin. The mixture was stirred for 2 h at room temperature, followed by dialysis of the final solution and washes with 10 mM PBS (details in *SI Materials and Methods*). The concentrated enzyme solution (stored at 4 °C) was used later for the preparation of enzyme solutions of different concentrations, using serial dilutions.

Biotinylation of Au Patterns, Enzyme Immobilization, and Particle Tracking. Au (90 nm) was patterned on a PEG-functionalized glass surface (MicroSurfaces), using an electron beam, with a 10-nm adhesion layer of Cr. Biotinylation of the circular Au patterns (radius = 3 mm) was achieved through the formation of a SAM, using a biotin–thiol linker (28) (preparation details in *SI Materials and Methods*). A solution of the linker in a solvent mixture of 1:1 H_2O:ethanol (8 mL of solution per milligram of biotin) was used for overnight incubation of the patterns at room temperature. After incubation, the patterns were washed several times with deionized water, followed by washes with 10 mM PBS buffer. The SAM-modified surfaces were then incubated in a streptavidin (ProZyme) solution (9 μM in 10 mM PBS) for 3 h, followed by incubation with enzyme–biotin solutions for 3–4 h before the experiments. The functionalized surfaces were washed with 10 mM PBS buffer after each incubation period to remove unbound material. Details of the experimental modifications of this procedure to control enzyme coverage are given in *SI Materials and Methods*.

Secure-seal hybridization chambers (Electron Microscopy Sciences) with dimensions of 20 mm diameter and 1.3 mm height were used to form closed-system devices, to which solutions of 500 mM urea in 10 mM PBS buffer solution were added. To monitor the fluid flow in all our experiments, 2 μm sulfate functionalized polystyrene microspheres (Polysciences Inc.) were introduced as tracers suspended in the substrate solution. Movies were captured using an optical setup composed of an inverted microscope (Zeiss Axiovert 200 MAT) with a halogen lamp (12 V max, 100 W) and a high-sensitivity Flea 3 USB 3 Digital Camera (FL3-U3-32S2C; Point Gray Research). To measure fluid pumping speed in each experiment, 30 tracer particles were tracked using Tracker (Open Source Physics and comPADRE). See *SI Materials and Methods* for tables of pumping speeds.

ACKNOWLEDGMENTS. We thank the Charles E. Kaufman Foundation for financial support. Partial funding was also provided by the National Science Foundation (NSF) under Materials Research Science and Engineering Center Grant DMR-1420620, by the Defense Threat Reduction Agency (HDTRA1-13-1-0039). I.O.-R. acknowledges a NSF Fellowship (DGE-1255832). A.C.B. acknowledges support from the Department of Energy under DOE Award DE-FG02 90ER45438.

1. Bănică F-G (2012) Enzymes and enzymatic sensors. *Chemical Sensors and Biosensors: Fundamentals and Applications* (John Wiley and Sons, Ltd., Chichester, UK), pp 28–49.
2. Sengupta S, et al. (2014) Self-powered enzyme micropumps. *Nat Chem* 6(5):415–422.
3. Zhang C, et al. (2015) Autonomic molecular transport by polymer films containing programmed chemical potential gradients. *J Am Chem Soc* 137(15):5066–5073.
4. Sengupta S, et al. (2014) DNA polymerase as a molecular motor and pump. *ACS Nano* 8(3):2410–2418.
5. Anderson JL (1989) Colloid transport by interfacial forces. *Annu Rev Fluid Mech* 21(1):61–99.
6. Chen PY, Keh HJ (2005) Diffusiophoresis and electrophoresis of a charged sphere parallel to one or two plane walls. *J Colloid Interface Sci* 286(2):774–791.
7. McDermott JJ, et al. (2012) Self-generated diffusioosmotic flows from calcium carbonate micropumps. *Langmuir* 28(44):15491–15497.
8. Reinmüller A, Schöpe HJ, Palberg T (2013) Self-organized cooperative swimming at low Reynolds numbers. *Langmuir* 29(6):1738–1742.
9. Pojman JA, Epstein IR (1990) Convective effects on chemical waves. 1. Mechanisms and stability criteria. *J Phys Chem* 94(12):4966–4972.
10. Muddana HS, Sengupta S, Mallouk TE, Sen A, Butler PJ (2010) Substrate catalysis enhances single-enzyme diffusion. *J Am Chem Soc* 132(7):2110–2111.
11. Lide DR (2005) *CRC Handbook of Chemistry and Physics* (CRC Press, Boca Raton, FL), 85th Ed.
12. Agar JN (1960) The rate of attainment of Soret equilibrium. *Trans Faraday Soc* 56(0): 776–787.
13. Braun D, Libchaber A (2002) Trapping of DNA by thermophoretic depletion and convection. *Phys Rev Lett* 89(18):188103.
14. Story MJ, Turner JCR (1969) Thermal diffusion of diphenyl in benzene and of urea in water. *Trans Faraday Soc* 65(0):1810–1811.
15. Busse FH (1978) Non-linear properties of thermal convection. *Rep Prog Phys* 41(12): 1929–1967.
16. Gershuni GZ, Zhukhovitskii EM (1963) On the convectional instability of a two-component mixture in a gravity field. *J Appl Math Mech* 27(2):441–452.
17. Gobin D, Bennacer R (1994) Double diffusion in a vertical fluid layer: Onset of the convective regime. *Phys Fluids* 6(1):59–67.
18. Rongy L, Goyal N, Meiburg E, De Wit A (2007) Buoyancy-driven convection around chemical fronts traveling in covered horizontal solution layers. *J Chem Phys* 127(11): 114710.
19. Basu AS, Gianchandani YB (2005) Trapping and manipulation of particles and droplets using micro-toroidal convection currents, in *Proceedings of IEEE Conference on Solid-State Sensors, Actuators and Microsystems* (IEEE, Piscataway, NJ), pp 85–88.
20. Liron N, Mochon S (1976) Stokes flow for a stokeslet between two parallel flat plates. *J Eng Math* 10(4):287–303.
21. Vanag VK, Epstein IR (2009) Cross-diffusion and pattern formation in reaction-diffusion systems. *Phys Chem Chem Phys* 11(6):897–912.
22. Aidun CK, Clausen JR (2010) Lattice-Boltzmann method for complex flows. *Annu Rev Fluid Mech* 42(1):439–472.
23. Ladd AJC, Verberg R (2001) Lattice-Boltzmann simulations of particle-fluid suspensions. *J Stat Phys* 104(5):1191–1251.
24. Guo Z, Zheng C, Shi B (2002) Discrete lattice effects on the forcing term in the lattice Boltzmann method. *Phys Rev E Stat Nonlin Soft Matter Phys* 65(4 Pt 2B):046308.
25. Mezrhab A, Bouzidi M, Lallemand P (2004) Hybrid lattice-Boltzmann finite-difference simulation of convective flows. *Comput Fluids* 33(4):623–641.
26. Shum H, Yashin VV, Balazs AC (2015) Self-assembly of microcapsules regulated via the repressilator signaling network. *Soft Matter* 11(18):3542–3549.
27. Cao L (2005) *Carrier-Bound Immobilized Enzymes: Principles, Application and Design* (Wiley-VCH Verlag GmbH, Weinheim, Germany).
28. Zimmermann RM, Cox EC (1994) DNA stretching on functionalized gold surfaces. *Nucleic Acids Res* 22(3):492–497.
29. Shum H, Gaffney EA (2015) Hydrodynamic analysis of flagellated bacteria swimming near one and between two no-slip plane boundaries. *Phys Rev E Stat Nonlin Soft Matter Phys* 91(3):033012.
30. Sengupta S, et al. (2013) Enzyme molecules as nanomotors. *J Am Chem Soc* 135(4): 1406–1414.